O(2×1)-Ag(110) missing-row reconstruction: Structure determination by low-energy ion scattering

M. Canepa, P. Cantini, F. Fossa, L. Mattera, and S. Terreni
Dipartimento di Fisica, Università di Genova, via Dodecaneso 33, 16146 Genova, Italy
(Received 13 November 1992)

Impact collision ion scattering spectroscopy using Ne^+ has been employed to determine the structure of the O(2×1)-Ag(110) phase. The analysis of experimental data by Monte Carlo simulation of the ion trajectories confirms the missing-row reconstruction with the formation of -Ag-O-Ag- chains (added rows) along the ⟨001⟩ direction. Oxygen is found to occupy the long-bridge site 0.03±0.08 Å below the silver atoms, while the first-to-second and the second-to-third interlayer spacings are 1.66±0.03 Å and 1.32±0.03 Å, respectively. A lateral displacement (0.08±0.03 Å) of the second-layer Ag atoms towards the missing rows is observed in addition to a vertical buckling in the third layer: the atoms lying under the missing rows are held about 0.08 Å above those positioned under the added rows.

I. INTRODUCTION

An impressive amount of theoretical and experimental work has been devoted in the last few years to the study of dissociative chemisorption of oxygen on the Ag(110) surface; the strong interest on this system is related to the catalytic activity that silver-based catalysts present for the ethylene epoxidation and methanol partial oxidation reactions.[1] Above 190 K, O_2 molecules dissociate on Ag(110) leading to the formation of well-ordered phases characterized by a $(n\times1)$ periodicity with $2\le n\le8$ (Refs. 2 and 3) and it is well established that oxygen atoms adsorb in the long-bridge site leading to the formation of -Ag-O-Ag- rows along the ⟨001⟩ azimuthal direction.

The phase at highest coverage ($n=2$) has been studied the most by several experimental techniques. Among these investigations, ion backscattering[4] (IS) and low-energy electron diffraction[5] experiments, which stimulated a long debate on the structure of the substrate, should be mentioned.

Recently, it was suggested that in the O(2×1)-Ag(110) phase oxygen adsorption would induce a missing-row reconstruction with the formation of added rows along the ⟨001⟩ direction, in close similarity with the O(2×1)-Cu(110) (Refs. 6–8) and O(2×1)-Ni(110) (Refs. 9–11) phases. An angle-resolved photoemission study[12] was able to exclude the unreconstructed model, but it could not discriminate between missing- and buckled-row reconstruction.

The missing-row model was strongly supported by a surface phonon investigation through thermal He inelastic scattering measurements[13] and it was confirmed by a subsequent surface-extended x-ray-absorption fine-structure (SEXAFS) study[14] that could not estimate independently the vertical position of adsorbed oxygen and the relaxation of Ag layers. More recently, scanning tunneling microscopy data[15] have indicated the presence of -Ag-O-Ag- added rows with a formation mechanism strictly similar to that observed for the O(2×1)-Cu(110) phase.[8]

Motivated by the fundamental relevance of adsorbate-induced surface reconstruction and its like connection with catalytic properties, we report in the present paper a structural study of the O(2×1)-Ag(110) phase performed by impact collision ion scattering spectroscopy (ICISS). ICISS has been widely employed in the study of surface structure mainly because of its surface sensitivity and its capability to give direct information on the structure of the first few layers of the sample.[16] At impact energies of a few keV, the ion-surface interaction can be treated as a sequence of two-body, classical, and elastic collisions which make the theoretical analysis conceptually simple. Furthermore, the large scattering angle (close to 180°) of the ICISS configuration strongly reduces the importance of multiple-scattering events, and structural information can be easily obtained from the measurement of critical angles defined through shadowing and focusing effects.[17]

Although more complex and time consuming, we have performed detailed calculations of ion-surface scattering as their comparison with the experimental data provide accurate information both on surface structure (geometry, disorder, and thermal motion of surface atoms) and ion-surface interaction (ion-atom potential, neutralization effects, and surface damaging induced by ion bombardment).

This paper is organized as follows. Experimental conditions and data are reported in Sec. II. The model calculations are described in Sec. III, their results are given in Sec. IV and discussed in Sec. V. Summary and conclusions are finally reported in Sec. VI.

II. EXPERIMENTAL

The experimental setup has been described previously in detail.[18] A noble-gas ion beam with energy up to 3 keV is produced in a differentially pumped source. The full angular divergency of the beam is 0.5°, the spot size on the sample is 1.5 mm (diameter), and the current density employed in the ICISS experiments is 1 nA/cm^2. Backscattered ions are detected by a channeltron multiplier after energy selection through an electrostatic analyzer

whose resolution is $\Delta E/E = 1\%$.

The sample is an Ag single crystal cut along the (110) surface within 0.5°. The surface is prepared by cycles of sputtering with Ne^+ at 3 keV followed by annealing at 750 K. In order to prepare the O(2×1) layer, the surface is exposed to an oxygen pressure of about 10^{-4} Torr while the sample temperature slowly decreases from 650 to 400 K. The layer periodicity is then tested at room temperature by thermal energy helium diffraction, a highly sensitive tool to check long-range surface order.[19] Diffraction peaks are sharp and stable for several hours, showing the presence of a stable, well-ordered phase.[3]

ICISS measurements have been performed at room temperature, using both He^+ and Ne^+ beams, along the ⟨001⟩, ⟨1$\bar{1}$0⟩, and ⟨1$\bar{1}$2⟩ directions at the fixed scattering angle of 155.0° ±0.2°. The backscattering intensity is measured as function of the polar angle of incidence ψ (measured with respect to the surface plane) from 0° to 90°.

The angular distribution measured with a He^+ beam ($E_0 = 2.9$ keV) along the ⟨1$\bar{1}$0⟩ direction is shown in Fig. 1. Data obtained with a Ne^+ beam at the same energy and along the same direction are shown in Fig. 2(b). A comparison between the two figures shows that a richer pattern is obtained with Ne^+. This behavior can be related to the higher neutralization probability experienced by He^+ with respect to Ne^+,[18] as already observed at these energies on many surfaces.[20]

We have decided, therefore, to work with a Ne^+ beam even though mass ratio and sputtering efficiency would have designated the He^+ species as being more appropriate for studying a low-mass adsorbate. This choice implies that the oxygen atoms cannot be observed directly as the Ne^+-O interaction does not provide any backscattered Ne^+ because of their mass ratio. It implies also that the analysis of the data taken along the ⟨001⟩ direction, where -Ag-O-Ag- chains are located, does not supply structural information as O atoms adsorbed in the long-bridge site between Ag atoms cannot be sampled and partially inhibit the observation of Ag-Ag focusing. Structural information on the O(2×1)-Ag(110) phase has been extracted from the distributions of Ne^+ backscattered from the ⟨1$\bar{1}$0⟩ and ⟨1$\bar{1}$2⟩ directions reported in Fig. 2.

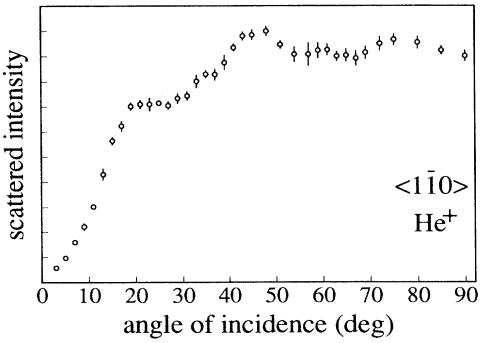

FIG. 1. He^+ backscattered intensity at $E_0 = 2.9$ keV along the ⟨1$\bar{1}$0⟩ direction.

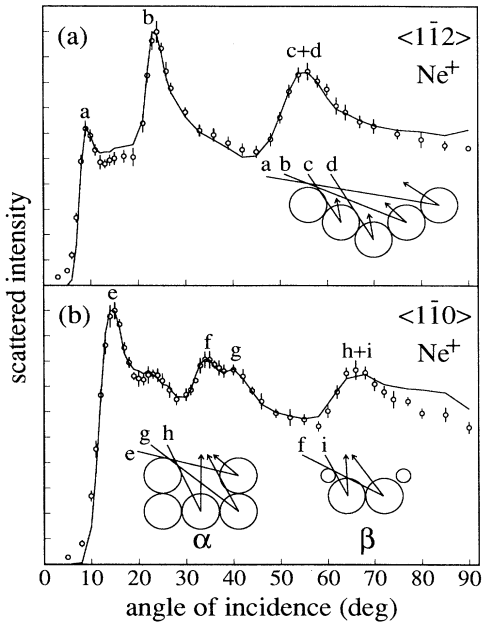

FIG. 2. Ne^+ backscattered intensity at $E_0 = 2.9$ keV along the ⟨1$\bar{1}$2⟩ (a) and ⟨1$\bar{1}$0⟩ (b) directions. The insets show schematically the Ag (large circles) and O (small circles) arrangement in a missing-row configuration. Letters on the curves identify focusing peaks due to trajectories shown in the insets. The continuous curve represents the best-fit calculations.

By taking advantage of the shadowing and focusing effects,[17] the occurrence of the focusing peaks in the spectra of Fig. 2 can be explained (all but one) in terms of the ion trajectories shown in the insets of the figure where the surface atoms are schematically positioned in a missing-row structure. This qualitative analysis is enough to conclude that oxygen adsorption induces a surface reconstruction. The incompatibility of the measured spectra with an unreconstructed surface can, in fact, be demonstrated by assuming an Ag atom positioned in the first layer, at the center of the inset of Fig. 2(a): the trajectories causing the focusing peaks marked "*a*" and "*b*" become impossible owing to the shadowing by this atom. An unreconstructed surface would give rise to a single peak at an intermediate angular position between *a* and *b*, as it occurs for the clean Ag(1$\bar{1}$0) surface.[18] Analogous considerations are valid for the focusing peaks marked by "*e*" and "*g*" in Fig. 2(b). With the same type of arguments it is, however, not easy to disregard the occurrence of a reconstruction of the buckled-row type. We discuss this at the end of Sec. V.

The presence of the small peak at 23° in the ⟨1$\bar{1}$0⟩ spectrum [Fig. 2(b)] cannot be explained in terms of either a missing- or a buckled-row scheme. This structure, is in fact, attributed to surface damage caused by ion bombardment as its intensity increases with the time of exposure to the ion beam while the intensities of all other peaks decrease. Furthermore, the polar scan on the bare Ag(110) surface taken along the ⟨1$\bar{1}$0⟩ direction in the same conditions shows a focusing peak just at 23°.[18]

In order to evaluate ion damage, the intensities of

peaks a and e [see Figs. 2(a) and 2(b)], characteristic of the (2×1) phase, were measured as a function of time. The intensity of these peaks decreases by about 20% after 20 min and this time interval was set as the maximum limit for the acquisition of a single scan. Once the scan is completed, the surface temperature is raised up to 700 K in order to desorb the residual oxygen and a new O(2×1) layer is prepared and checked by He diffraction. The diffraction patterns which are measured on distinct layers are indistinguishable ensuring a good reproducibility of the preparation method.

The spectra reported in Figs. 2(a) and 2(b) are obtained by averaging over 16 scans on distinct layers, the error bar representing the standard deviation of the value distribution at each angle of incidence. All spectra are measured starting from $\psi=0°$ in order to reduce surface damage in the region at low angle where significant structures occur.

III. ION-SURFACE INTERACTION MODEL

Data analysis is performed by a Monte Carlo simulation of in-plane ion trajectories using a computational model which has been successfully applied to the study of the Ag(110) surface in a previous work.[18] In the model, an ion-surface atom potential is adopted and the thermal motion of crystal atoms, the ion neutralization probability, and the ion-induced damaging effects are taken into account. Furthermore, the effects of the finite spot and of the angular divergency of the ion beam, of the crystal dimension, and of the acceptance and energy resolution of the detector are also accounted for.

A. Ion-atom potential

Ion-surface scattering is treated as a sequence of two-body classical interactions described by the Thomas-Fermi-Molière-Firsov (TFMF) potential[21]

$$V(r)=\frac{Z_1Z_2e^2}{r}\chi\left[\frac{r}{Ca_{\mathrm{TF}}}\right], \tag{1}$$

where the screening function $\chi(x)$ in the Molière approximation is given by

$$\chi(x)=0.35e^{-0.3x}+0.55e^{-1.2x}+0.10e^{-6.0x}$$

and the Firsov screening length

$$a_{\mathrm{TF}}=\frac{0.885a_0}{[Z_1^{1/2}+Z_2^{1/2}]^{2/3}}$$

(a_0 is the Bohr radius) is multiplied by the adjustable parameter C (screening parameter).

In the sequence of collisions Ne^+ can interact with the O and Ag atoms so that both the Ne^+-O and the Ne^+-Ag potentials must be considered. For the Ne^+-Ag potential the value of $C=0.8$ has been accurately determined.[18] This value has been used in many other works to treat the interaction of Ne^+ with different atoms, such as Ni,[22] Cu,[6] and Au,[23] and it has also been adopted here for the Ne^+-O potential;[6] this choice will be further discussed in Sec. V.

Ion trajectories, with starting points uniformly distributed over the surface cell, are followed during the sequence of collisions until they eventually enter the detector slit. The ions are finally counted provided that their energy matches the energy window of the analyzer. Up to 2×10^7 trajectories per angle of incidence are considered.

B. Thermal motion

Thermal effects are modeled by considering a static disorder with surface atoms randomly displaced from their equilibrium sites according to a Gaussian distribution.[24] For both Ag and O atoms, the same root-mean-square displacement $\sigma=0.12$ Å,[18] obtained from Ag(110) clean-surface data, has been used. The good agreement between the angular width of the calculated and experimental focusing peaks shows this treatment of thermal motion to be correct also for O(2×1)-Ag(110).

C. Ion neutralization

Neutralization processes are taken into account through the ion survival probability[25,26]

$$P=1-P_n=\exp(-t_e/t_n), \tag{2}$$

where t_e is the time the ion spends below a reference plane during its trajectory in and out of the surface. The position of this plane h_n measured with respect to the topmost layer (positive direction is towards the vacuum) and the lifetime t_n of the ions under this plane are free parameters. The model then assumes a uniform probability for the ion to be neutralized in the region below h_n. Since neutralization is proportional to the electron density[27] of the sample, this is equivalent to assuming a step-like shape of the electron density in the z direction normal to the surface.

D. Ion-induced surface damage

Surface damage is taken into account by assuming that it produces, on a fraction of the surface, a perfect phase (damage phase) different from the original O(2×1). The backscattering intensity $I(\psi)$ is then calculated as

$$I(\psi)=[1-f(\psi)]I_{\mathrm{O}}(\psi)+f(\psi)I_d(\psi), \tag{3}$$

where $I_{\mathrm{O}}(\psi)$ and $I_d(\psi)$ are the intensities relative to the O(2×1) phase and the damage phase, respectively. The fraction $f(\psi)$ of the damage phase can be calculated from

$$\frac{df}{dt}=g(\psi)\sin\psi(1-f), \tag{4}$$

where the term $\sin\psi$ takes into account the variation with the angle of incidence of the ion-beam current density.

In Eq. (4), $g(\psi)$ gives the incoming ion probability to damage the O(2×1) phase (desorption, sputtering, displacement from site, etc.) which, in a simple model, has been assumed to be proportional to $1/\sin\psi$,[28] although experimental data on sputtering yields[29] would have suggested a slightly stronger angular dependence. Thus, on

integrating Eq. (4),

$$f=1-\exp(-t/\tau) \tag{5}$$

is obtained. In Eq. (5), τ is the lifetime of the O(2×1) phase and the angular dependence appears only through the experimentally known correspondence between the angle of incidence ψ and the exposure time t. As mentioned in the previous section, each polar scan is performed starting from $\psi=0°$ so that surface damage gets larger as ψ and time increase. $I_d(\psi)$ has been calculated for several oxygen phases of decreasing coverage on Ag(110) and for the bare surface. These results will be discussed in Sec. IV and V.

IV. DATA ANALYSIS

The surface structure of the O(2×1) phase is determined by applying the computational model described in the previous section to the experimental data of Fig. 2. Concerning the focusing peaks in the figure, it is useful to recall that (i) the angular positions are determined by surface geometry, (ii) the relative intensities are related to surface geometry and neutralization effects, and (iii) the angular widths are related to surface geometry, thermal motion of sample atoms, and neutralization effects. In the calculations structural and neutralization parameters were varied in order to obtain the best fit to the experimental data in both the $\langle 1\bar{1}0\rangle$ and $\langle 1\bar{1}2\rangle$ azimuthal directions. These structural parameters are illustrated in Fig. 3 where top and side views of the surface in a missing-row structure are shown. Note that along the $\langle 1\bar{1}0\rangle$ direction two nonequivalent planes, α and β, only one of them (β) containing oxygen atoms, must be taken into account in two-dimensional calculations.

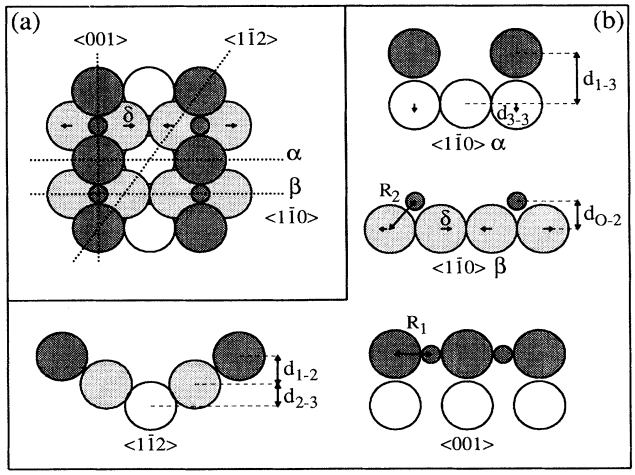

FIG. 3. Top view (a) and side views (b) of the O(2×1)-Ag(110) surface in the missing-row reconstruction. Small circles, oxygen atoms; large circles, silver atoms. Dark grey, topmost layer; light grey, second layer; white, third layer.

A. $\langle 1\bar{1}2\rangle$ azimuthal direction

In order to fit the measured intensities, the neutralization model described in Sec. III was slightly modified. In an open structure such as that occurring in the $\langle 1\bar{1}2\rangle$ direction, a single reference plane is not adequate as it would introduce too crude an averaging of the electron density. Two reference planes were then introduced at heights h_1 and h_2 with respect to the topmost layer. The planes define two regions: *outer* (between h_1 and h_2) and *inner* (below h_2), characterized by different ion lifetimes, t_1 and t_2, respectively. The best-fit parameters are $h_1=1.2$ Å, $h_2=-1.6$ Å and $t_1=15$ fs, $t_2=2.4$ fs. Note that the negative value implies that h_2 lies below the topmost layer. As expected, t_2 (inner region) is smaller than t_1 (outer region) because of an increase of the electron density effective in the ion neutralization process.

The angular positions of the focusing peaks at 24° (b) and 56° ($c+d$) in Fig. 2(a) are related to the first-to-second and second-to-third interlayer spacings [$d_{1\text{-}2}$ and $d_{2\text{-}3}$, respectively, in Fig. 3(b)] and to the lateral displacement of the Ag atoms in the second layer along the $\langle 1\bar{1}0\rangle$ direction (δ in Fig. 3). The comparison between experimental and calculated data normalized to the absolute maximum is reported in Fig. 4. The dashed line in the figure represents the calculated intensity assuming bulklike interlayer spacings ($d_{1\text{-}2}=d_{2\text{-}3}=1.44$ Å) without lateral displacement ($\delta=0$) and in the absence of ion damaging. The position of "a" is correctly reproduced but the focusing peaks "b" and "$c+d$" occur at angles smaller than the measured ones. To shift b to larger angles the $d_{1\text{-}2}$ spacing must be increased, and this also shifts c in the right direction. However, to reproduce the entire spectrum in Fig. 4 we need to reduce $d_{2\text{-}3}$ from the bulk value and introduce the displacement δ (see Fig. 3).

The best agreement with the experimental data (full line in Fig. 4) has been found assuming $d_{1\text{-}2}=1.66\pm0.03$ Å, $d_{2\text{-}3}=1.32\pm0.03$ Å, and $\delta_{\langle 1\bar{1}2\rangle}=0.045$ Å, the projection of δ along the $\langle 1\bar{1}2\rangle$ direction. The determination of δ will be discussed in the data analysis of the $\langle 1\bar{1}0\rangle$ direction where damage effects, which have so far been

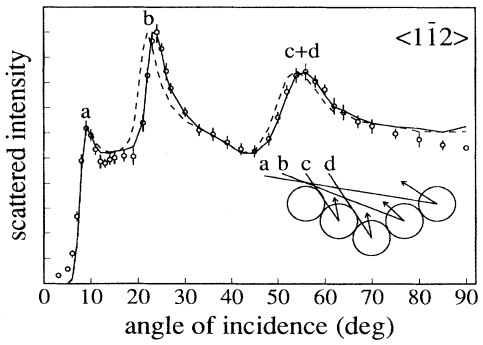

FIG. 4. Comparison between calculated (without damaging) and experimental data along $\langle 1\bar{1}2\rangle$. Dashed line, bulklike parameters ($\delta=0$); full line, parameters from Table I, $\delta_{\langle 1\bar{1}2\rangle}=0.045$ Å.

TABLE I. Structural parameters. See Fig. 3 for parameter definition; all distances are in Å. The bulk interlayer distance is 1.44 Å.

	$d_{1\text{-}2}$	$d_{2\text{-}3}$	$d_{3\text{-}3}$	δ	$d_{O\text{-}1}$
O(2×1)[a]	1.66±0.03	1.32±0.03	0.08±0.04	0.08±0.03	−0.03±0.08
Ag(110)[b]	1.38±0.03	1.46±0.04			

[a]Added-row reconstructed surface.
[b]Unreconstructed (Ref. 18).

neglected, will also be considered. Here, as in the following, uncertainties in the fitting parameters are determined from experimental error bars.

B. ⟨1$\bar{1}$0⟩ azimuthal direction

To analyze experimental data taken along the ⟨1$\bar{1}$0⟩ direction [Fig. 2(b)] scattering processes occurring in both planes α and β in Fig. 3 have to be considered. Damaging also has to be taken into account as the structure measured at $\psi \simeq 23°$ cannot be ascribed to any of the trajectories shown in the inset of Fig. 2(b).

In plane α, besides the spacing of Ag atoms in the first layer determining the peak "*e*," the angular position of peaks "*g*" and "*h*" are determined by the distances $d_{1\text{-}3}$ and $d_{3\text{-}3}$, respectively. The former gives the first-to-third layer separation and the latter defines the buckling of Ag atoms in the third layer under the added row, with respect to the Ag atom under the missing row in the same layer (see Fig. 3). $d_{1\text{-}3}$ was determined from the data along the ⟨1$\bar{1}$2⟩ direction and it is held at $d_{1\text{-}3}=d_{1\text{-}2}+d_{2\text{-}3}=2.98$ Å while $d_{3\text{-}3}$ is determined by fitting to the shape of the decaying part of *g*.

The geometry of plane β determines the positions of peaks "*f*" and "*i*" through the lateral displacement δ and the vertical position of oxygen atoms $d_{O\text{-}2}$ measured with respect to the Ag atoms in the second layer. Both $d_{O\text{-}2}$ and δ affect the angular positions of the peaks near 35° and 65°, but in a different way: on changing δ these peaks are displaced in opposite directions, while on varying $d_{O\text{-}2}$ they shift in the same direction.

In α and β, the structure is compact so that a single reference plane is expected to be adequate to describe the neutralization effects. The values of the neutralization parameters are found to be $h_n=0.5$ Å and $t_n=3.5$ fs for both α and β.

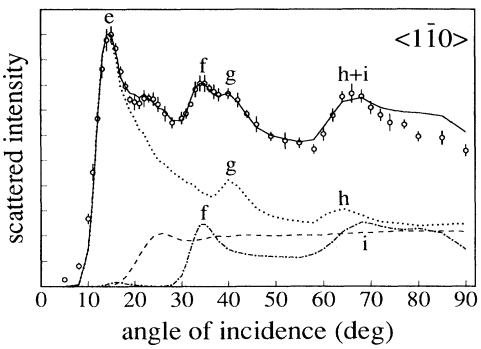

FIG. 5. Comparison between calculated and experimental data along ⟨1$\bar{1}$0⟩. Dotted line, contribution from plane α (see Fig. 3); dashed-dotted line, contribution from plane β; dashed line, contribution from the clean Ag(110) fraction; full line, sum of all contributions. For structural parameters see Table I.

As discussed in the previous section, ion-induced damage is accounted for by considering the contribution to the scattered intensity from a damage phase [Eqs. (3)–(5)]. By comparison with the Ag(110) data,[18] the occurrence of a peak at $\psi \simeq 23°$ suggests that ion damage produces a fraction of the clean surface on the sample. Ag(110) is then assumed to be the damage phase and the scattered intensity is calculated as

$$I_{\langle 1\bar{1}0\rangle}=\tfrac{1}{2}[1-f][I_\alpha+I_\beta]+fI_{\mathrm{Ag}(110)}\ , \tag{6}$$

where f is given by Eq. (5), and I_α, I_β, and $I_{\mathrm{Ag}(110)}$ are the intensities relative to planes α, β, and Ag(110), respectively. Structural and neutralization parameters from Ref. 18 are adopted to describe the Ag(110) fraction ($d_{1\text{-}2}=1.38$ Å, $d_{2\text{-}3}=1.46$ Å, $h_n=1.24$ Å, and $t_n=5.1$ fs). The results of the calculations are shown in Fig. 5 where the contributions of I_α, I_β, and $I_{\mathrm{Ag}(110)}$ to $I_{\langle 1\bar{1}0\rangle}$ [see Eq. (6)] are reported for the best-fit values of $d_{O\text{-}2}$ and δ given in Table I, and $\tau=50$ min [see Eq. (5)].

V. DISCUSSION

The agreement between the experimental and calculated data is excellent both with respect to peak position and intensity on either ⟨1$\bar{1}$0⟩ and ⟨1$\bar{1}$2⟩ azimuthal directions (see Figs. 4 and 5). The major discrepancy is present along ⟨1$\bar{1}$0⟩ (Fig. 5) towards normal incidence where the calculated intensities are larger than the experimental data. This angular region corresponds to ion trajectories passing close to oxygen atoms (see plane β in Fig. 3) where a higher electron density and therefore a higher neutralization probability has to be expected. The discrepancy can then be ascribed to the neutralization model adopted which assumes a uniform probability for the ion to get neutralized in the region below h_n.

Several parameters enter in the analysis of the data. However, the values of these parameters are not arbitrary since each one of them controls a specific feature in the spectra.

As an example of the sensitivity of the calculation to a particular parameter, we show in Fig. 6 the effect of δ on the features measured along ⟨1$\bar{1}$0⟩ for angles of incidence between 30° and 60°. The full line is our best-fit curve with $\delta=0.08$ Å, while the dashed line refers to $\delta=0$. This lateral displacement δ of Ag atoms in the second layer, along ⟨1$\bar{1}$0⟩ (see Fig. 3), also induces some out-of-plane contributions to the scattering along ⟨1$\bar{1}$2⟩.

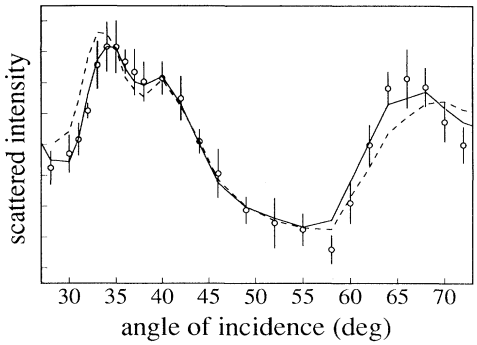

FIG. 6. Comparison of experimental data along $\langle 1\bar{1}0 \rangle$, with best-fit calculations (full line; see Fig. 5 and Table I) and calculations assuming $\delta=0$ (dashed line).

The good agreement with the experimental data of Fig. 4 and the consistency of the results in both azimuthal directions show, however, that it is sufficient to consider only in-plane scattering even along $\langle 1\bar{1}2 \rangle$ provided the projection of δ along that direction is accounted for ($\delta_{\langle 1\bar{1}2 \rangle}=0.045$ Å).

With regard to the determination of the vertical position of oxygen atoms, it should be pointed out that there is an uncertainty in the choice of the screening parameter C. Here, all calculations have been performed with $C=0.8$ for both the Ne^+-O and Ne^+-Ag potentials. This choice is supported by the experimental evidence that C is determined mainly by the incoming ion[31] but its value has never been determined directly for the Ne^+-O interaction. Assuming, for instance, that $C=0.7$, the same agreement between experimental and calculated data is obtained provided that the vertical position of oxygen atoms with respect to the second layer $d_{O\text{-}2}$ is raised from 1.63 to 1.68 Å. Taking into account this uncertainty in the screening parameter ($C=0.8\pm0.1$), we conclude that the oxygen atoms are 0.03 ± 0.08 Å below the silver atoms along the -Ag-O-Ag- chains.

The damage model considered for the $\langle 1\bar{1}0 \rangle$ direction was applied also to the $\langle 1\bar{1}2 \rangle$ data and the results are reported as a full line in Fig. 2(a). A comparison with Fig. 4 shows that damaging does not much affect the spectrum along this azimuth. Along this direction, the clean-surface fraction in the damaging model does introduce some contributions in the angular regions around $\psi\simeq15°$ and $\psi\simeq55°$.[18] However, these contributions are difficult to disentangle. The former is, in fact, located at a small angle of incidence corresponding to short exposure time to ion bombardment while the latter mixes with a focusing peak of the O(2×1) phase.

The treatment of ion-induced damage deserves some further comments. Because of the sputtering of oxygen atoms, damaging could create domains of $(n\times1)$ periodicity with $n\geq3$ instead of the clean-surface ones that have been assumed so far. Calculations have also been performed for $n=3$ assuming that even this phase is characterized by an added-row reconstruction.[30] The first focusing peak at small angles of incidence shifts to lower angles (the distance between Ag atoms in the first layer increases) without the occurrence of an adequate contribution at $\psi\simeq23°$. The same behavior also applies to phases characterized by a $n>3$ periodicity. This reinforces the idea that ion damaging does produce an area of clean surface: each ion that strikes the surface causes atomic disorder and oxygen removal in a small area around the impact point; thermal motion then induces a clean surface *deconstruction* in the area that has been deprived of oxygen on a time scale shorter than the experimental one.

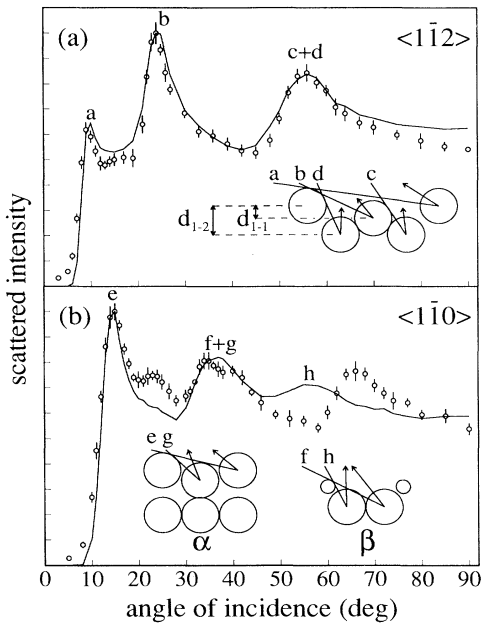

FIG. 7. Comparison of experimental data with calculations (full lines) performed for a buckled-row structure schematically shown in the insets ($d_{1\text{-}2}=1.90$ Å; $d_{1\text{-}1}=0.80$ Å).

From the current density of the incoming ion beam and the lifetime of the O(2×1) phase ($\tau=50$ min) it can be estimated that each incoming ion induces, on the average, the removal of 20 oxygen atoms creating a clean area of the order of 40 unit cells. Obviously, this is only a crude estimate but it seems to indicate the occurrence of a local heating of the sample upon ion impact.

To test the possibility of other reconstruction models, the buckled-row model was also investigated and the results (without considering damaging) are shown in Fig. 7. A quite strong buckling is necessary to allow the a and e focusing on the $\langle 1\bar{1}2 \rangle$ and $\langle 1\bar{1}0 \rangle$ directions, respectively. The data in the $\langle 1\bar{1}2 \rangle$ direction are then reasonably well reproduced while along $\langle 1\bar{1}0 \rangle$ this model definitely gives wrong results. Figure 7 also shows that, as in the case of the added-row reconstruction, the peak at $\psi\simeq23°$ cannot be reproduced if damaging is not taken into account.

VI. SUMMARY AND CONCLUSIONS

The O(2×1)-Ag(110) phase shows a surface reconstruction according to the added-row model. This model, in fact, was able to reproduce well the ICISS experimental data along the $\langle 1\bar{1}0 \rangle$ and $\langle 1\bar{1}2 \rangle$ azimuth with respect

to both angular positions and intensity of the focusing peaks leading to the determination of a set of uncoupled structural parameters which describe the first three layers of the sample. The detailed calculations have significantly reduced the uncertainty on the vertical position of adsorbed oxygen with respect to previous investigations.

An inspection of Table I shows that the -Ag-O-Ag- added rows are relaxed outward quite strongly. The presence of oxygen atoms reduces the second-to-third interlayer spacing $d_{2\text{-}3}$ both with respect to the $d_{1\text{-}2}$ and the $d_{2\text{-}3}$ distances of the clean Ag(110) surface, the former being the proper distance to compare with in the case of an added-row model. Ag atoms in the second layer are displaced, along the $\langle 1\bar{1}0 \rangle$ direction, towards the missing rows ($\delta = 0.08 \pm 0.03$ Å) and the Ag atoms in the third layer below the missing rows are shifted upward of 0.08 ± 0.04 Å with respect to neighbor atoms along $\langle 1\bar{1}0 \rangle$ in the same layer.

The oxygen atom adsorbs in the long-bridge site and its vertical position is 0.03 ± 0.08 Å below the Ag atoms of the added row, in good agreement with the earlier IS determination of Ref. 4. The reported error is ascribed mainly to the uncertainty about the screening parameter C [Eq. (1)] of the Ne^+-O interaction potential.

In order to compare the present findings with the results of a recent SEXAFS study[14] on the same phase, the distances R_1 and R_2 between the oxygen atom and its nearest and next-nearest neighbor (Fig. 3) have been calculated. The values $R_1 = 2.045 \pm 0.005$ Å and $R_2 = 2.23 \pm 0.08$ Å are in excellent agreement with $R_1 = 2.05 \pm 0.03$ Å and $R_2 = 2.21 \pm 0.03$ Å of Ref. 14.

The detailed calculations of the scattered intensity have provided information also on ion neutralization and surface damaging. Ion-induced damage has to be taken into account to correctly reproduce scattered intensity particularly along the $\langle 1\bar{1}0 \rangle$ direction. The simple model introduced here indicates that each ion impinging on the surface induces removal, on the average, of 20 oxygen atoms. Ion-induced damage reduces oxygen coverage and produces areas of clean Ag(110). The formation of phases of higher periodicity [$O(n \times 1), n \geq 3$] seems to be excluded as this model could not fit the experimental data. Since it is well known that oxygen chains interact repulsively, it can be concluded that the chains are broken and *holes* of the clean surface are formed.

ACKNOWLEDGMENTS

The authors wish to thank G. Bracco and T. S. Rahman for helpful discussions. We acknowledge support from the Centro di Fisica delle Superfici e Basse Temperature del CNR and the Consorzio INFM.

[1] M. A. Barteau and R. J. Madix, in *The Chemical Physics of Solid Surfaces and Heterogeneous Catalysis,* edited by D. A. King and D. P. Woodruff (North-Holland, Amsterdam, 1982), Vol. 4.
[2] H. A. Engelhardt and D. Menzel, Surf. Sci. **57**, 591 (1976).
[3] M. Canepa, P. Cantini, L. Mattera, S. Terreni, and F. Valdenazzi, Phys. Scr. T **41**, 226 (1992).
[4] W. Heiland, F. Iberl, E. Taglauer, and D. Menzel, Surf. Sci. **53**, 383 (1975).
[5] E. Zanazzi, M. Maglietta, U. Bardi, F. Jona, and P. M. Marcus, J. Vac. Sci. Technol. A **1**, 7 (1983).
[6] H. Dürr, Th. Fauster, and R. Schneider, Surf. Sci. **244**, 237 (1991), and references therein.
[7] S. R. Parkin, H. C. Zeng, M. Y. Zhou, and K. A. R. Mitchell, Phys. Rev. B **41**, 5432 (1990).
[8] D. J. Coulman, J. Wintterlin, R. J. Behm, and G. Ertl, Phys. Rev. Lett. **64**, 1761 (1990); Y. Kuk, F. M. Chua, P. J. Silverman, and J. A. Meyer, Phys. Rev. B **41**, 12 393 (1990).
[9] H. Bu, C. D. Roux, and J. W. Rabalais, J. Chem. Phys. **97**, 1465 (1992).
[10] G. Kleinle, J. Wintterlin, G. Ertl, R. J. Behm, F. Jona, and W. Moritz, Surf. Sci. **225**, 171 (1990).
[11] F. Besenbacher, I. Stensgaard, L. Ruan, J. K. Nørskov, and K. W. Jacobsen, Surf. Sci. **272**, 334 (1992).
[12] L. H. Tjeng, M. B. J. Meinders, and G. A. Sawatzky, Surf. Sci. **236**, 341 (1990).
[13] L. Yang, T. S. Rahman, G. Bracco, and R. Tatarek, Phys. Rev. B **40**, 12 271 (1989).
[14] L. Becker, S. Aminpirooz, A. Schmalz, B. Hillert, M. Pedio, and J. Haase, Phys. Rev. B **44**, 13 655 (1991).
[15] T. Sakurai, T. Hashizume, and S. Hyodo, Prog. Theor. Phys. Suppl. **106**, 387 (1991); M. Taniguchi, K. Tanaka, T. Hashizume, and T. Sakurai, Surf. Sci. **262**, L123 (1992).
[16] M. Aono, Nucl. Instrum. Methods B **2**, 374 (1984).
[17] R. Souda, M. Aono, C. Oshima, S. Otani, and Y. Ishizawa, Surf. Sci. **179**, 199 (1987).
[18] G. Bracco, M. Canepa, P. Cantini, F. Fossa, L. Mattera, S. Terreni, and D. Truffelli, Surf. Sci. **269/270**, 61 (1992).
[19] B. Poelsema and G. Comsa, in *Scattering of Thermal Energy Atoms,* edited by G. Höhler, Springer Tracts in Modern Physics Vol. 115 (Springer-Verlag, Berlin, 1989).
[20] W. Eckstein, V. A. Molchanov, and H. Verbeek, Nucl. Instrum. Methods **149**, 599 (1978).
[21] I. M. Torrens, *Interatomic Potentials* (Academic, New York, 1982).
[22] T. M. Buck, I. Stensgaard, and G. H. Wheatley, Nucl. Instrum. Methods **170**, 519 (1980).
[23] J. Möller, H. Niehus, and W. Heiland, Surf. Sci. **166**, L111 (1986).
[24] R. Souda, M. Aono, C. Oshima, S. Otani, and Y. Ishizawa, Surf. Sci. **128**, L236 (1983).
[25] R. S. Daley and R. S. Williams, J. Vac. Sci. Technol. A **6**, 808 (1988).
[26] B. J. Garrison, Surf. Sci. **87**, 683 (1979).
[27] H. D. Hagstrum, Phys. Rev. **96**, 336 (1954).
[28] D. T. Goldman and A. Simon, Phys. Rev. **111**, 383 (1958).
[29] H. H. Andersen and H. L. Bay, in *Sputtering by Particle Bombardment I,* edited by R. Behrisch (Springer-Verlag, Berlin, 1981).
[30] G. Bracco, R. Tatarek, and G. Vandoni, Phys. Rev. B **42**, 1852 (1990).
[31] C. S. Chang, U. Knipping, and I. S. T. Tsong, Nucl. Instrum. Methods B **18**, 11 (1986).